Editors' Suggestion

Direct Observation of Full-Gap Superconductivity and Pseudogap in Two-Dimensional Fullerides

Ming-Qiang Ren,[1] Sha Han,[1] Shu-Ze Wang,[1] Jia-Qi Fan,[1] Can-Li Song,[1,2,*] Xu-Cun Ma,[1,2,†] and Qi-Kun Xue[1,2,3,‡]

[1]State Key Laboratory of Low-Dimensional Quantum Physics, Department of Physics, Tsinghua University, Beijing 100084, China

[2]Frontier Science Center for Quantum Information, Beijing 100084, China

[3]Beijing Academy of Quantum Information Sciences, Beijing 100193, China

(Received 23 December 2019; accepted 15 April 2020; published 5 May 2020)

Alkali-fulleride superconductors with a maximum critical temperature $T_c \sim 40$ K exhibit a similar electronic phase diagram to that of unconventional high-T_c superconductors. Here we employ cryogenic scanning tunneling microscopy to show that trilayer K_3C_{60} displays fully gapped strong coupling s-wave superconductivity, accompanied by a pseudogap above $T_c \sim 22$ K and within vortices. A precise control of the electronic correlations and potassium doping enables us to reveal that superconductivity occurs near a superconductor-Mott-insulator transition and reaches maximum at half-filling. The s-wave symmetry retains over the entire phase diagram, which, in conjunction with an abrupt decline of the superconductivity below half-filling, indicates that alkali fullerides are predominantly phonon-mediated superconductors, although the electronic correlations also come into play.

DOI: 10.1103/PhysRevLett.124.187001

Trivalent fullerides A_3C_{60} (A = alkali metals) have historically been, albeit not universally [1,2], thought of as conventional Bardeen-Cooper-Schrieffer (BCS) superconductors [3–5]. However, several recent experiments revealed a dome-shaped dependence of T_c on interfullerene separation and a proximate magnetic Mott-insulating state [6–10], which bear a striking resemblance to those of the unconventional high-T_c superconductors from cuprates to ferropnictides [11,12]. This highlights the importance of electronic correlations in fulleride superconductors [13,14]. Therefore, alkali fullerides represent a unique family of superconductors, in which a conventional phonon-mediated superconductivity encounters with Mott physics [15]. Because of air sensitivity and phase separation of A_3C_{60}, experiments on fulleride superconductors have been mostly conducted by nuclear magnetic resonance and magnetization measurements [6–10]. A direct visualization of the superconducting state in alkali fullerides is quite rare [16]. The microscopic mechanism of fulleride superconductivity with the conventional phonon-mediated pairing [4,5] or unconventional electronic pairing [1,2,6,7,13], or a synergy between them [9,14,17], remains controversial.

Unlike cuprates, which superconduct through the two-dimensional (2D) CuO_2 planes [18], alkali fullerides are attributed to the three-dimensional (3D) members of the high-T_c family [13,14]. An interplay between electronic correlations and molecular Jahn-Teller (JT) instability might reduce the dimensionality of low-lying states from 3D to 2D [19–21]. This matches with the high upper critical field of 90 T observed near the superconductor-Mott-insulator transition (SMIT) in $Rb_xCs_{3-x}C_{60}$ [22]. A fundamental question thus arises naturally as to how the reduced dimensionality affects the superconductivity in fullerides [23], or whether the superconductivity survives down to the 2D limit.

Our experiments were performed in an ultrahigh vacuum cryogenic (down to 2.5 K) scanning tunneling microscopy (STM), which is connected to a molecular beam epitaxy (MBE) system for *in situ* sample preparation. Fullerene C_{60} molecules grow layer-by-layer on graphitized SiC(0001) substrates, followed by controlled potassium (K) doping, with details in the Supplemental Material [24]. Polycrystalline PtIr tips were used after calibration on Ag/Si(111) films. All STM topographies were taken in a constant current mode. Tunneling dI/dV spectra and maps were acquired using a standard lock-in technique with a modulation frequency $f = 975$ Hz, while the modulation amplitudes were 0.2 and 20 meV for measuring the superconducting gaps and wider-energy-range (± 1.0 eV) dI/dV spectra, respectively.

As schematically drawn in Figs. 1(a) and 1(b), epitaxial K_xC_{60} ($x \sim 3$) films crystallize into a face-centered cubic (fcc) structure, demonstrated in Supplemental Material, Sec. 2 [24]. Figure 1(c) show an STM topography of trilayer K_3C_{60}, presenting unreconstructed and C_{60}-terminated (111)-1 × 1 surface (white rhombus). In marked contrast with bulk fcc fullerides [6,8], the tri-lobe-like C_{60} molecules (with one hexagon pointing up) in epitaxial K_3C_{60} films have the same orientation and exhibit no orientational (merohedral) disorder [25]. The closely packed C_{60} molecules are spaced 10.0 ± 0.1 Å apart, comparable to the reported value of 10.07 Å in bulk K_3C_{60} [4].

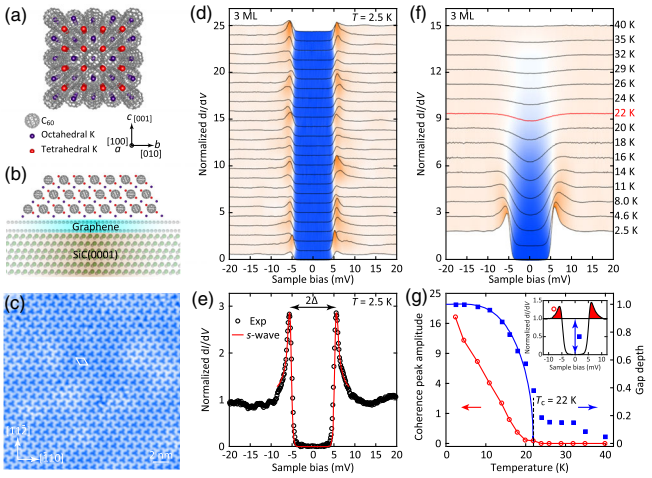

FIG. 1. (a) Crystal structure of fcc K_3C_{60}. The purple and red spheres denote K dopants at the octahedral and tetrahedral sites, respectively. (b) Schematic (side) view of $K_3C_{60}(111)$ films on graphitized SiC(0001) substrate. (c) STM topography ($V = 1.0$ V, $I = 10$ pA) of trilayer K_3C_{60}. (d) Grid dI/dV spectra (5 pixels × 5 pixels) in a field of view of 20 nm× 20 nm. The set point is stabilized at $V = 20$ mV and $I = 200$ pA, unless otherwise specified. For comparison, each dI/dV spectrum is normalized to a cubic background by fitting the raw conductance beyond the superconducting gap ($|V| > 10$ mV). This normalization procedure is used throughout. (e) The dI/dV spectrum and its best fit (red curve) to a single isotropic s-wave superconducting gap with $\Delta = 5.4$ meV. (f) Spatially averaged tunneling spectra as a function of temperature, presenting a pseudogap above $T_c = 22$ K (red curve). (g) Measured dependence on temperature of coherence peak amplitude (circles) and gap depth (squares), defined as the integration over red-shaded areas and difference between unity and the normalized zero-energy conductance $\sigma_{0,N}$ (see inset), respectively.

Figure 1(d) shows the spatial dependence of the tunneling conductance spectra $\sigma(E = eV) \equiv dI/dV$ in trilayer K_3C_{60} at 2.5 K (E is the electron energy), which measures the quasiparticle density of states (DOS) and superconducting gap at Fermi energy (E_F). Despite some heterogeneity in the coherence peaks, the quasiparticle DOS in dI/dV spectra vanishes completely over an extended energy range $|E| \leq 4.5$ meV, indicating a fully gapped superconductivity. At some positions, the gap exhibits pronounced coherence peaks and could be fairly well fitted with a single BCS-type isotropic s-wave gap function [Fig. 1(e)] [16]. The mean gap magnitude Δ, half the distance between the two coherence peaks, is estimated to be 5.7 ± 0.3 meV. Figure 1(f) plots the temperature dependence of the superconducting gap from 2.5 to 40 K, which is gradually suppressed at elevated temperatures, as anticipated. However, a corresponding analysis of the normalized tunneling dI/dV spectra as a function of temperature in Fig. 1(g) reveals an anomaly in gap depth (blue squares) around 22 K that we refer to as T_c, at which the coherence peaks coincidentally disappear (red circles). Across T_c, the superconducting gap evolves continuously into a normal state quasiparticle gap with an energy scale that changes little with temperature. This is reminiscent of the pseudogap phenomena in the underdoped cuprates [26,27], where the pseudogap just becomes smeared out with increasing temperature above T_c.

Intriguingly, only a triple layer K_3C_{60} sustains a pseudogap and an s-wave superconductivity with both T_c and Δ exceeding those ($T_c \sim 19$ K, $\Delta = 4.4$ meV) of its bulk counterpart [16,28,29]. Such findings have been unambiguously corroborated by the observation of vortices under magnetic field B [Fig. 2(a)]. By fitting the radial dependence of the normalized zero-energy conductance $\sigma_{0,N}$ in the vicinity of magnetic vortices (Supplemental Material, Sec. 3 [24]), the superconducting coherence length ξ is deduced and found to be azimuthal angle θ-independent [Figs. 2(b) and 2(c)]. This is consistent with the isotropic s-wave symmetry in K_3C_{60}, since $\xi \propto 1/\Delta$ in BCS theory. The mean $\xi = 2.6 \pm 0.5$ nm matches well with that ($\xi \sim 2.6$ nm) in bulk K_3C_{60} [30]. Plotted in Fig. 2(d) are a series of tunneling spectra across a vortex core at 2 T. Vortices suppress the coherence peaks but a pseudogap remains (red line). No bound states are induced in the vortex cores. We emphasize that the pseudogap exists within all vortices we investigated at varied B (Supplemental Material, Sec. 3 [24]), and ought to be inherent to trilayer K_3C_{60}. In contrast to cuprates [27], no spatially modulated electronic charge density is observed in trilayer K_3C_{60} and the

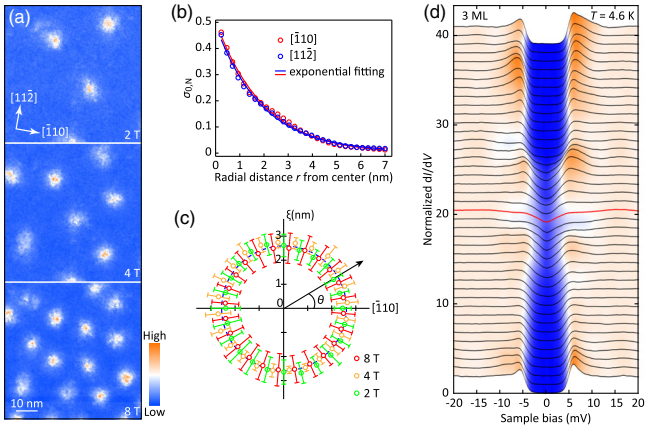

FIG. 2. (a) Spatial maps (300 pixels × 300 pixels) of zero-energy conductance $\sigma_0(V = 0)$, revealing vortices (i.e., the orange and white regions with enhanced σ_0) at $B = 2$, 4, and 8 T in the same field of view of 63 nm × 63 nm. (b) Vortex-induced $\sigma_{0,N}$ versus the radial distance r from the center of a vortex at 8 T. Solid lines are the best exponential fits ($\sigma_{0,N} \sim e^{-r/\xi}$), giving the superconducting coherence length of ξ. (c) Azimuthal dependence of $\xi(\theta)$. The statistical errors of ξ indicate the standard derivations of $\xi(\theta)$ obtained for different vortices at a given magnetic field. (d) Tunneling spectra measured at $T = 4.6$ K and $B = 2$ T along a 20-nm trajectory across a vortex core in trilayer K_3C_{60}. The red line indicates a pseudogap at the vortex center.

bulk counterpart [31], a fact which supports the notion that charge density wave (CDW) correlations are not responsible for the opening of the pseudogap in high-T_c superconductors. This issue continues to be an important point of contention [32–34].

To shed light on the enhanced superconductivity and pseudogap in trilayer K_3C_{60}, we explore the layer-dependent structural and electronic properties of K-doped fullerides. Unlike trilayer K_3C_{60}, both monolayer and bilayer ones display $\sqrt{3} \times \sqrt{3}$ superstructures, as marked by the colored rhombuses in Figs. 3(a) and 3(b). Figure 3(c) depicts the spatially averaged dI/dV spectra at varied K_3C_{60} layers. Note that the 9 ML-thick K_3C_{60} exhibits a metal-like electronic DOS with two sharp peaks below and above E_F, which follows the calculated electronic DOS profile for fully ordered K_3C_{60} [35]. This not only hints at merohedral disorder-free K_3C_{60}, as observed, but also suggests a similarity of the band structure between the 9 ML and bulk K_3C_{60}. As the layer is reduced, a dip or insulating gap is noticeable near E_F and increases in size [Fig. 3(c)], hallmarks of a metal-insulator transition. The observed tunneling gaps of a few hundreds of meV are too large to be ascribed to possible CDW correlations, associated with the $\sqrt{3} \times \sqrt{3}$ superstructures in monolayer and bilayer K_3C_{60}. We propose that the gaps arise from the enhanced electronic correlations due to the poor screening of K_3C_{60} at the 2D limit [Fig. 3(d)]. A strong Coulomb repulsion U, assisted by JT effects, splits the t_{1u}-derived band of C_{60} into subbands [36]. The half-filled K_3C_{60} therefore becomes a Mott-JT insulator (MJTI) with charge gap opening near E_F, as the Cs_3C_{60} behaves at ambient pressure [7–9]. By measuring U between the upper Hubbard bands (UHB, marked by red triangles) and lower Hubbard bands (LHB, marked by blue triangles) in Fig. 3(c) and the band width W (Supplemental Material, Sec. 4 [24]), one sees that U/W reduces with a K_3C_{60} layer [Fig. 3(d)], prompting a layer-controlled SMIT ($U/W \sim 1$) between trilayer and bilayer K_3C_{60}. The trilayer K_3C_{60} exists on the verge of SMIT and a small enhancement of U renders the bilayer K_3C_{60} nonsuperconducting (Supplemental Material, Sec. 5 [24]). Here the reduced U in multilayer K_3C_{60} is distinct from a previous report of fulleride films on Au(111) [25], owing to the different substrates used [36].

A similar SMIT has previously been identified in Cs_3C_{60} and $Rb_xCs_{3-x}C_{60}$ ($0.35 \leq x < 2$) through a continuous control of W, tuned by the interfullerene separation [6–9]. Alternatively, the SMIT observed in this study is governed by the dimension-controlled U [Fig. 3(d)]. Figure 3(e) represents the temperature-dependent dI/dV spectra on 9 ML K_3C_{60}. At 2.5 K, the spectrum features an s-wave superconducting gap as well, whereas $\Delta = 4.8 \pm 0.2$ meV and $T_c \sim 18.4$ K [Fig. 3(f)] appear smaller than those of trilayer K_3C_{60}. More remarkably, the pseudogap remains above T_c and within vortices [Figs. 3(e) and 3(g)], but gets suppressed in thicker 9 ML K_3C_{60} [Fig. 3(h)]. Given its nonobservability in bulk fullerides [16,31], our results imply that pseudogap might be a general phenomenology of 2D superconductors [37].

Next, we examine the superconductivity of K_xC_{60} as the electron doping deviates from half-filling by tuning the stoichiometry. This enables us to track for the first time the variations of Δ and T_c over a wide range of electron

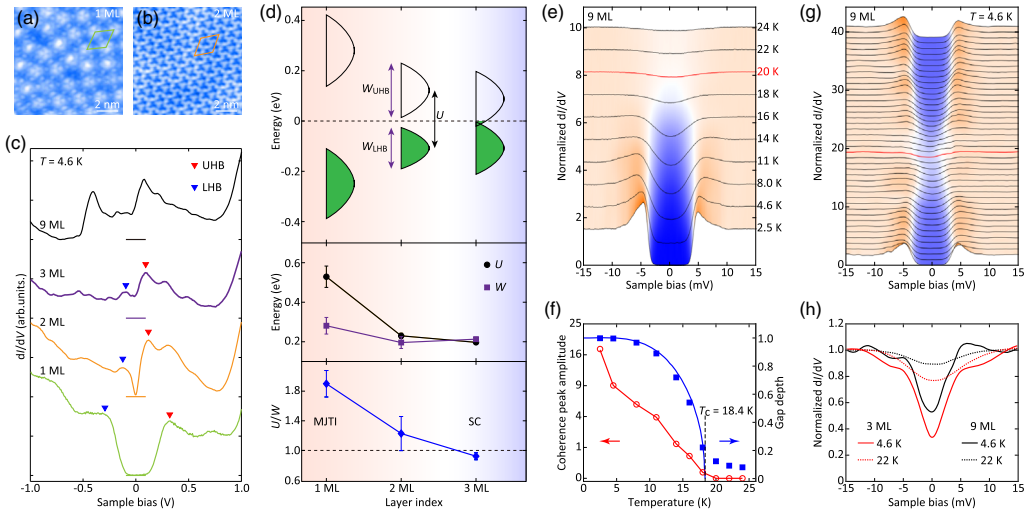

FIG. 3. (a),(b) STM topographies of monolayer and bilayer K_3C_{60} ($V = 1.0$ V, $I = 10$ pA). (c) Layer-dependent tunneling dI/dV spectra over a wide energy range of ± 1.0 eV. Set point: $V = 1.0$ V and $I = 100$ pA. (d) Schematic energy bands (top panel) with only the UHB (unfilled) and LHB (green) shown, measured Hubbard U, W (middle panel) and U/W (lower panel) of K_3C_{60} as a function of layer index. The statistical errors indicate the standard derivations of U and W measured in various regions. (e),(f) Temperature-dependent tunneling spectra of 9 ML K_3C_{60}, revealing a mild pseudogap (red curve) above $T_c = 18.4$ K. (g) Conductance spectra measured at $T = 4.6$ K and $B = 2$ T along a 20-nm trajectory across a vortex core in 9 ML K_3C_{60}. Red line marks the dI/dV curve at vortex center. (h) Pseudogaps at 4.6 K (measured within vortices) and 22 K.

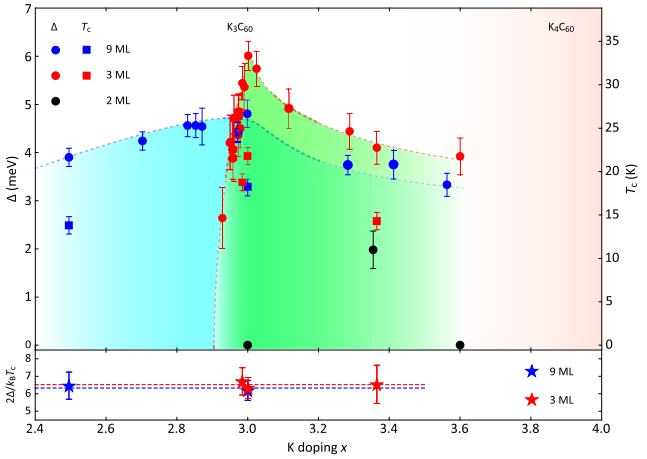

FIG. 4. Electronic phase diagram showing the evolution of T_c (squares), Δ (solid circles), and reduced gap $2\Delta/k_BT_c$ (stars, lower panel) at 4.6 K, as a function of K doping x. Colored symbols distinctively mark the K_xC_{60} films at varied layer (2, black; 3, red; 9 ML, blue). Gradient shading from green (cyan) to white schematically draws the superconducting dome of 3 ML (9 ML) K_xC_{60} with a peaked T_c and Δ at $x = 3$. Dashed lines correspond to the experimental tracks for Δ and $2\Delta/k_BT_c$. The T_c has an uncertainty of 1.0 K and the statistical errors of $x < 0.5$ are smaller than the symbol size.

doping (x) from 2.5 to 3.6 at varied U (Supplemental Material, Secs. 4 and 6 [24]). In Fig. 4, we draw the Δ (circles) and T_c (squares) *versus* x electronic phase diagram. Apparently, Δ scales with T_c (lower panel) and exhibits dome-shaped variations with maxima at half-filling. A minor but significant distinction between 3 and 9 ML fullerides is that the superconductivity in trilayer K_xC_{60} decreases very abruptly below half-filling. Above $x \sim 3.6$, an insulating phase characteristic of tetravalent fullerides emerges and becomes dominant at $x = 4$ (Supplemental Material, Sec. 6) [24,38,39].

The unusual phase diagram reveals important aspects of the high-T_c superconductivity in fulleride solids. First, the superconductivity declines smoothly as the electron doping x deviates from half-filling in 9 ML K_xC_{60}. This finding contrasts sharply with an early study [40], where a conclusive evolution of T_c with doping was frustrated by the sample diversity with and without merohedral disorders, and is not necessarily contradictory to the BCS-Eliashberg theory of phonon-mediated superconductivity. However, we find it is nontrivial to understand the superconducting domes solely from x-dependent DOS variation at E_F [5], because the electronic DOS of half-filled K_3C_{60} shows a shoulder and even minimum at E_F [Fig. 3(c)]. The DOS (E_F) and superconductivity would be enhanced as $x > 3$, at odds with what we reveal. We therefore speculate that if the BCS-Eliashberg theory is applicable to fulleride superconductors, either phonon spectrum or electron-phonon coupling or both should vary substantially with doping. This merits further experimental investigations.

Second, it seems unlikely that the Δ shrinkage is due to some form of disorder effects away from half-filling, as the $\Delta \sim x$ evolution is essentially layer dependent and of great asymmetry relative to $x = 3$ in trilayer fullerides. Another possible explanation of the dome-shaped superconductivity is associated with the x-dependent electronic correlations [14]. Given the fact that the electronic DOS and correlations rely crucially on the K_xC_{60} layer (Supplemental Material, Sec. 4 [24]), there exists little opportunity that Δ coincidentally reaches its maximum at half-filling in both 3 and 9 ML fullerides. In any case, the electronic phase diagram unambiguously rules out the scenario that fulleride superconductivity results from an accidental doping of A_3C_{60} [1].

A view of fulleride superconductors that has received increasing attention is that the electron-phonon coupling and electronic correlations together bring about the high-T_c superconductivity [9,14,17]. Within this and related pictures, it has been theoretically revealed that T_c (or Δ) drops slowly away from half-filling for small U/W, which agrees qualitatively with our finding in 9 ML K_xC_{60}. However, this model fails to account for the dome asymmetry and steep $\Delta(x)$ reduction below half-filling in trilayer K_xC_{60} (a variation of x by ~0.1 almost kills the superconductivity), due to its oversimplification. In reality, the electronic correlations reduce with x (Supplemental Material, Sec. 4 [24]). Therefore, a possible cause of the dome asymmetry in trilayer fullerides might be that the enhanced electronic correlations localize electrons and significantly suppress superconductivity below half-filling. Nevertheless, the s-wave symmetry retains over the entire phase diagram [Fig. S8] [24], suggesting a phonon-mediated electron pairing in fullerides irrespective of U. A primary role of electronic correlations may be that they increase the quasiparticle mass and decrease W, leading to an increase of the electronic DOS at E_F. This is most probably the cause of enhanced superconductivity in trilayer K_3C_{60} films. It is worth noting that the phonon-mediated s-wave superconductivity has also been evidenced in other carbon-based superconductors such as intercalated graphite [41,42].

As a final remark, we comment on the reduced gap $2\Delta/k_BT_c > 6$ [Fig. 4] that exceeds both of the canonical BCS value of 3.53 and that (5.3) of bulk K_3C_{60} in tunneling experiments [16]. This suggests an extremely strong-coupling superconductivity and matches nicely with the enhanced U in K_xC_{60} films, since $2\Delta/k_BT_c$ was found to rise abruptly close to the Mott transition in fulleride superconductors [9,43,44]. It thus becomes an important future issue to study theoretically how strong correlations are reconcilable to a robust s-wave symmetry over the entire phase diagram of fulleride superconductors. Another interesting experimental challenge is to access tunable high-T_c superconductivity down to the monolayer limit by increasing W (i.e., using smaller Na or Li as dopants) or reducing U (see the superconductivity of overdoped bilayer $K_{3.37}C_{60}$ in Supplemental Material, Sec. 5 [24]). In contrast

to fcc A_3C_{60} bulk crystals, the stoichiometric K_3C_{60} film is merohedrally ordered, suffering from no structural and chemical complexity. This appears important as it offers an ideal material for understanding superconductivity in strongly correlated electron systems that is conclusively of *s*-wave symmetry in fullerides.

This work was financially supported by the Ministry of Science and Technology of China (2017YFA0304600, 2018YFA0305603, 2016YFA0301004), the Natural Science Foundation of China (Grants No. 11634007, No. 11427903, and No. 11774192), and in part by the Beijing Advanced Innovation Center for Future Chip (ICFC).

*clsong07@mail.tsinghua.edu.cn
†xucunma@mail.tsinghua.edu.cn
‡qkxue@mail.tsinghua.edu.cn

[1] R. W. Lof, M. A. van Veenendaal, B. Koopmans, H. T. Jonkman, and G. A. Sawatzky, Phys. Rev. Lett. **68**, 3924 (1992).
[2] M. Capone, M. Fabrizio, C. Castellani, and E. Tosatti, Science **296**, 2364 (2002).
[3] M. Schluter, M. Lannoo, M. Needels, G. A. Baraff, and D. Tománek, Phys. Rev. Lett. **68**, 526 (1992).
[4] O. Gunnarsson, Rev. Mod. Phys. **69**, 575 (1997).
[5] A. Ceulemans, L. F. Chibotaru, and F. Cimpoesu, Phys. Rev. Lett. **78**, 3725 (1997).
[6] A. Ganin, Y. Takabayashi, Y. Khimyak, S. Margadonna, A. Tamai, M. Rosseinsky, and K. Prassides, Nat. Mater. **7**, 367 (2008).
[7] Y. Takabayashi, A. Ganin, P. Jeglic, D. Arcon, T. Takano, Y. Iwasa, Y. Ohishi, M. Takata, N. Takeshita, K. Prassides, and M. Rosseinsky, Science **323**, 1585 (2009).
[8] A. Ganin, Y. Takabayashi, P. Jeglič, D. Arcon, A. Potočnik, P. Baker, Y. Ohishi, M. McDonald, M. Tzirakis, A. McLennan, G. Darling, M. Takata, M. Rosseinsky, and K. Prassides, Nature (London) **466**, 221 (2010).
[9] R. Zadik, Y. Takabayashi, G. Klupp, R. Colman, A. Ganin, A. Potočnik, P. Jeglič, D. Arčon, P. Matus, K. Kamarás, Y. Kasahara, Y. Iwasa, A. Fitch, Y. Ohishi, G. Garbarino, K. Kato, M. Rosseinsky, and K. Prassides, Sci. Adv. **1**, e1500059 (2015).
[10] P. Durand, G. Darling, Y. Dubitsky, A. Zaopo, and M. Rosseinsky, Nat. Mater. **2**, 605 (2003).
[11] B. Keimer, S. A. Kivelson, M. R. Norman, S. Uchida, and J. Zaanen, Nature (London) **518**, 179 (2015).
[12] Y. Takabayashi and K. Prassides, Phil. Trans. R. Soc. A **374**, 20150320 (2016).
[13] M. Capone, M. Fabrizio, C. Castellani, and E. Tosatti, Rev. Mod. Phys. **81**, 943 (2009).
[14] Y. Nomura, S. Sakai, M. Capone, and R. Arita, Sci. Adv. **1**, e1500568 (2015).
[15] Y. Nomura, S. Sakai, M. Capone, and R. Arita, J. Phys. Condens. Matter **28**, 153001 (2016).
[16] Z. Zhang, C. C. Chen, and C. Lieber, Science **254**, 1619 (1991).
[17] J. E. Han, O. Gunnarsson, and V. H. Crespi, Phys. Rev. Lett. **90**, 167006 (2003).
[18] Y. J. Yu, L. G. Ma, P. Cai, R. D. Zhong, C. Ye, J. Shen, G. D. Gu, X. H. Chen, and Y. B. Zhang, Nature (London) **575**, 156 (2019).
[19] G. Klupp, P. Matus, K. Kamarás, A. Ganin, A. McLennan, M. Rosseinsky, Y. Takabayashi, M. McDonald, and K. Prassides, Nat. Commun. **3**, 912 (2012).
[20] S. Hoshino and P. Werner, Phys. Rev. Lett. **118**, 177002 (2017).
[21] S. Hoshino, P. Werner, and R. Arita, Phys. Rev. B **99**, 235133 (2019).
[22] Y. Kasahara, Y. Takeuchi, R. Zadik, Y. Takabayashi, R. Colman, R. McDonald, M. Rosseinsky, K. Prassides, and Y. Iwasa, Nat. Commun. **8**, 14467 (2017).
[23] D. Erbahar, D. Liu, S. Berber, and D. Tománek, Phys. Rev. B **97**, 140505(R) (2018).
[24] See Supplemental Material at http://link.aps.org/supplemental/10.1103/PhysRevLett.124.187001 for details on film preparation, pseudogap, filling-controlled electronic DOS, and superconductivity of K-doped fullerides.
[25] Y. Y. Wang, R. Yamachika, A. Wachowiak, M. Grobis, and M. Crommie, Nat. Mater. **7**, 194 (2008).
[26] C. Renner, B. Revaz, J.-Y. Genoud, K. Kadowaki, and O. Fischer, Phys. Rev. Lett. **80**, 149 (1998).
[27] Ø. Fischer, M. Kugler, I. Maggio-Aprile, C. Berthod, and C. Renner, Rev. Mod. Phys. **79**, 353 (2007).
[28] A. Hebard, M. Rosseinsky, R. Haddon, D. Murphy, S. Glarum, T. Palstra, A. Ramirez, and A. Kortan, Nature (London) **350**, 600 (1991).
[29] P. W. Stephens, L. Mihaly, P. L. Lee, R. L. Whetten, S.-M. Huang, R. Kaner, F. Deiderich, and K. Holczer, Nature (London) **351**, 632 (1991).
[30] K. Holczer, O. Klein, G. Gruner, J. D. Thompson, F. Diederich, and R. L. Whetten, Phys. Rev. Lett. **67**, 271 (1991).
[31] H. Alloul, P. Wzietek, T. Mito, D. Pontiroli, M. Aramini, M. Riccò, J. P. Itie, and E. Elkaim, Phys. Rev. Lett. **118**, 237601 (2017).
[32] S. Caprara, C. Di Castro, G. Seibold, and M. Grilli, Phys. Rev. B **95**, 224511 (2017).
[33] B. Loret, N. Auvray, Y. Gallais, M. Cazayous, A. Forget, D. Colson, M.-H. Julien, I. Paul, M. Civelli, and A. Sacuto, Nat. Phys. **15**, 771 (2019).
[34] M. Bluschke, M. Yaari, E. Schierle, G. Bazalitsky, J. Werner, E. Weschke, and A. Keren, Phys. Rev. B **100**, 035129 (2019).
[35] M. P. Gelfand and J. P. Lu, Phys. Rev. Lett. **68**, 1050 (1992).
[36] S. Han, M. X. Guan, C. L. Song, Y. L. Wang, M. Q. Ren, S. Meng, X. C. Ma, and Q. K. Xue, Phys. Rev. B **101**, 085413 (2020).
[37] C. Richter, H. Boschker, W. Dietsche, E. Fillis-Tsirakis, R. Jany, F. Loder, L. Kourkoutis, D. Muller, J. Kirtley, C. Schneider, and J. Mannhart, Nature (London) **502**, 528 (2013).
[38] N. Iwahara and L. F. Chibotaru, Nat. Commun. **7**, 13093 (2016).
[39] A. Isidori, M. Berović, L. Fanfarillo, L. de' Medici, M. Fabrizio, and M. Capone, Phys. Rev. Lett. **122**, 186401 (2019).
[40] T. Yildirim, L. Barbedette, J. E. Fischer, C. L. Lin, J. Robert, P. Petit, and T. Palstra, Phys. Rev. Lett. **77**, 167 (1996).

[41] T. E. Weller, M. Ellerby, S. S. Saxena, R. P. Smith, and N. T. Skipper, Nat. Phys. **1**, 39 (2005).

[42] N. Bergeal, V. Dubost, Y. Noat, W. Sacks, D. Roditchev, N. Emery, C. Hérold, J.-F. Marêché, P. Lagrange, and G. Loupias, Phys. Rev. Lett. **97**, 077003 (2006).

[43] A. Potočnik, A. Krajnc, P. Jeglič, Y. Takabayashi, A. Ganin, K. Prassides, M. Rosseinsky, and D. Arcon, Sci. Rep. **4**, 4265 (2015).

[44] P. Wzietek, T. Mito, H. Alloul, D. Pontiroli, M. Aramini, and M. Ricco, Phys. Rev. Lett. **112**, 066401 (2014).